Journal of Superconductivity and Novel Magnetism (2019) 32:2437–2446
https://doi.org/10.1007/s10948-018-4964-5

ORIGINAL PAPER

Synthesis, Characterization, and Magnetic Properties of $A_2Co_2Fe(VO_4)_3$ (A = Ag or Na) Alluaudite-Type Vanadates

Mohammed Hadouchi[1] · Abderrazzak Assani[1] · Mohamed Saadi[1] · Abdelilah Lahmar[2] · Mimoun El Marssi[2] · Mohammed Sajieddine[3] · Lahcen El Ammari[1]

Received: 3 November 2018 / Accepted: 3 December 2018 / Published online: 8 December 2018

Abstract
We successfully synthesized the polycrystalline form of vanadates $A_2Co_2Fe(VO_4)_3$ (A = Ag or Na) using sol–gel method. Powder X-ray diffraction analysis allowed the identification of the alluaudite-type vanadate structure. The morphology and the elemental composition of the synthesized powders were analyzed by scanning electron microscopy (SEM) and energy-dispersive X-ray spectrometer (EDS). The two vanadates $A_2Co_2Fe(VO_4)_3$ (A = Ag or Na) were further characterized by infrared and Raman spectroscopies to get complementary structural information. The infrared and Raman spectroscopy-observed bands were assigned to VO_4^{3-} vibration modes. The room temperature ^{57}Fe Mössbauer spectroscopy confirmed the +III oxidation state of iron. Magnetic properties of these vanadates were investigated. The magnetic susceptibility data reveal that the predominant interactions in these vanadates are antiferromagnetic with a Curie–Weiss constant of $\theta = -125.6$ K for $Na_2Co_2Fe(VO_4)_3$ and $\theta = -104.5$ K for $Ag_2Co_2Fe(VO_4)_3$. The magnetic interactions in these vanadates were discussed according to semiempirical Goodenough–Kanamori–Anderson rules (GKA).

Keywords Vanadate · Alluaudite-type structure · Magnetic properties · Powder X-ray diffraction · Mössbauer spectroscopy

1 Introduction

The research in the field of open-framework inorganic materials has extended dramatically during the last decades due to their promising applications in many fields, e.g., effective electrode materials for rechargeable batteries [1, 2], catalysis [3], and photocatalysis [4]. Also, transition metal-based inorganic materials with open frameworks have extensively investigated for their interesting magnetic properties [5, 6].

Following the comprehensive development of synthetic inorganic materials, research has gradually shifted towards the exploration of new families of compounds based on transition metals and exhibiting three-dimensional frameworks. Although, a family of phosphates named "alluaudite" [7] has attracted much attention during the last years [8–12].

The alluaudite mineral first known as phosphates, exhibiting a three-dimensional open framework, was first described by Fisher in 1955 [13], and its structure was studied by Moore in 1971 [7]. To date, numerous studies on alluaudite type phosphates have been stated such as their structural studies [8, 14–16], their magnetic properties, and their electrochemical performance as electroactive materials for rechargeable Na and Li-ion batteries [17–22]. Furthermore, alluaudite-type compounds are no longer limited to just the phosphates. Recent research has revealed that arsenates [23, 24], sulfates [25], and more recently vanadates [26–28] can also crystallize in alluaudite-type structure. Moreover, the ability of alluaudite-like structures to accommodate a wide selection of transition metals suggests the presence of interesting magnetic properties [22, 29, 30]. To the best of our knowledge, no magnetic properties of alluaudite-type vanadate have been reported.

In this context, as a continuation of our previous work reported on the structural study of $A_2Co_2Fe(VO_4)_3$ (A = Ag

✉ Mohammed Hadouchi
hadouchimohammed@yahoo.com

[1] Laboratoire de Chimie Appliquée des Matériaux, Centre des Sciences des Matériaux, Faculty of Sciences, Mohammed V University in Rabat, Avenue Ibn Battouta, BP 1014, Rabat, Morocco

[2] Laboratoire de Physique de La Matière Condensée (LPMC), Université de Picardie Jules Verne, Amiens, France

[3] Laboratoire de Physique des Matériaux, Faculté des Sciences et Techniques, Université Sultan Moulay Slimane, BP 523, 23000 Beni-Mellal, Morocco

or Na) [26], we report in this paper the sol–gel synthesis of the powder of these two vanadates and their characterization by powder X-ray diffraction and electron microprobe microscopy. Also, these vanadates were analyzed by IR, Raman, and ^{57}Fe Mössbauer spectroscopies. The magnetic properties of this vanadate are also discussed.

2 Experimental Section

2.1 Synthesis of $A_2Co_2Fe(VO_4)_3$ (A = Ag or Na)

$A_2Co_2Fe(VO_4)_3$ (A = Ag or Na) were synthesized by sol–gel method. In a first step, a stoichiometric proportion corresponding to desired composition of the reactants $AgNO_3$ or $NaNO_3$, $(CH_3COO)_2Co$, $4H_2O$, $Fe(NO_3)_3{\cdot}9H_2O$, and V_2O_5 was dissolved in appropriate amount of distilled water and a few drops of HNO_3 and kept under stirring. Secondly, citric acid was added to the mixture with a molar ratio of (Na/Ag + Fe + Co + V):citric acid = 1:4. The solution was evaporated slowly to form a viscous liquid which was kept under heating to dryness. The resulting gel was transferred to furnace to undergo successive heat treatments at 200, 400, 500, and finally at 540 °C for $Ag_2Co_2Fe(VO_4)_3$ and until 580 °C for $Na_2Co_2Fe(VO_4)_3$ with intermittent grinding. The duration of each treatment was 24 h. Black powders were obtained and their purity was confirmed by powder X-ray diffraction.

2.2 Characterizations

2.2.1 Scanning Electron Microscopy and Powder X-Ray Diffraction

The morphology and elemental analysis of the synthesized powders was performed by JEOL JSM-IT100 InTouchScope™ scanning electron microscope equipped with energy-dispersive X-ray spectroscopy analyzer (EDS).

To control the purity of the synthesized powders, X-ray powder diffraction patterns were obtained at room temperature using a Siemens D5000 powder diffractometer operating with θ–2θ scan mode and Cu Kα radiation ($\lambda = 1.5406$ Å). The data were collected over the 2θ angle range of $10° \leq 2\theta \leq 70°$ with a step size of 0.04° and 30 s per step counting time.

2.2.2 IR and Raman Spectroscopy

Raman spectroscopy data were collected using Renishaw in Via Qontor Raman microscope with 532 nm laser as excitation wavelength. Laser power has been optimized (0.5 mW) to avoid overheating of the sample. The spectrum was recorded in backscattering geometry from 50 to 1300 cm^{-1}.

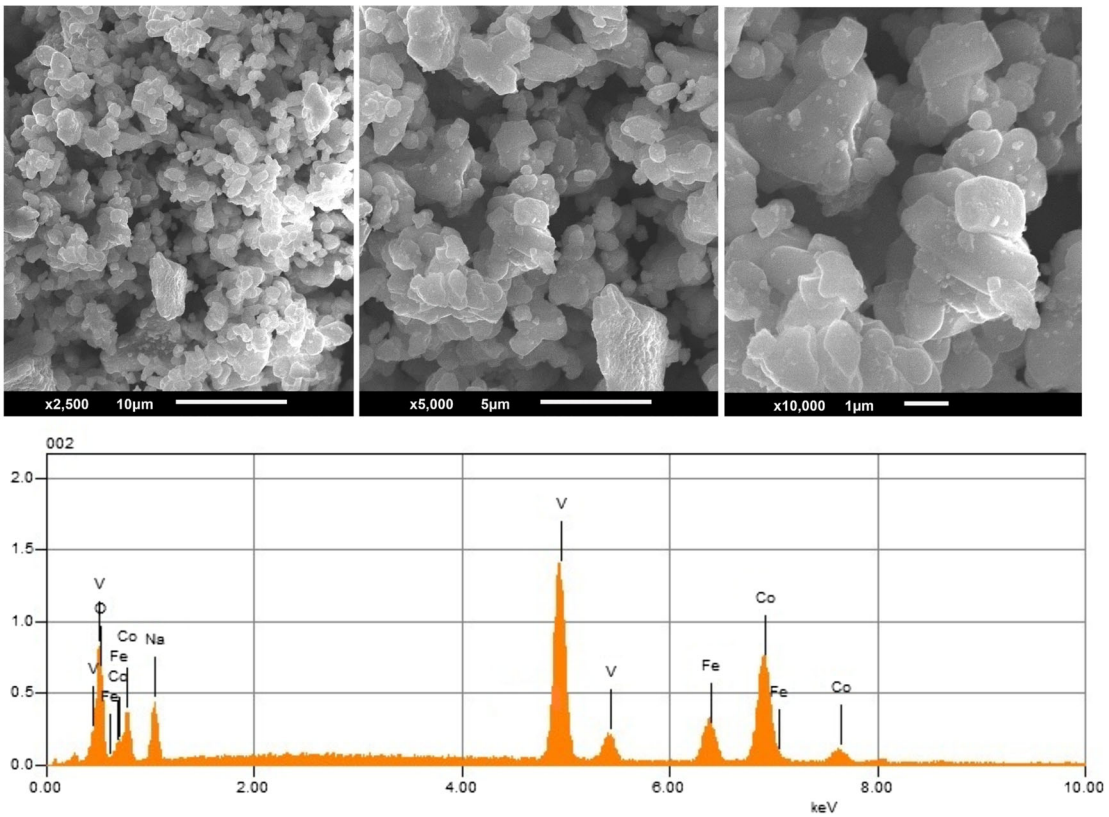

Fig. 1 SEM micrographs and EDS spectrum of the synthesized powder of $Na_2Co_2Fe(VO_4)_3$

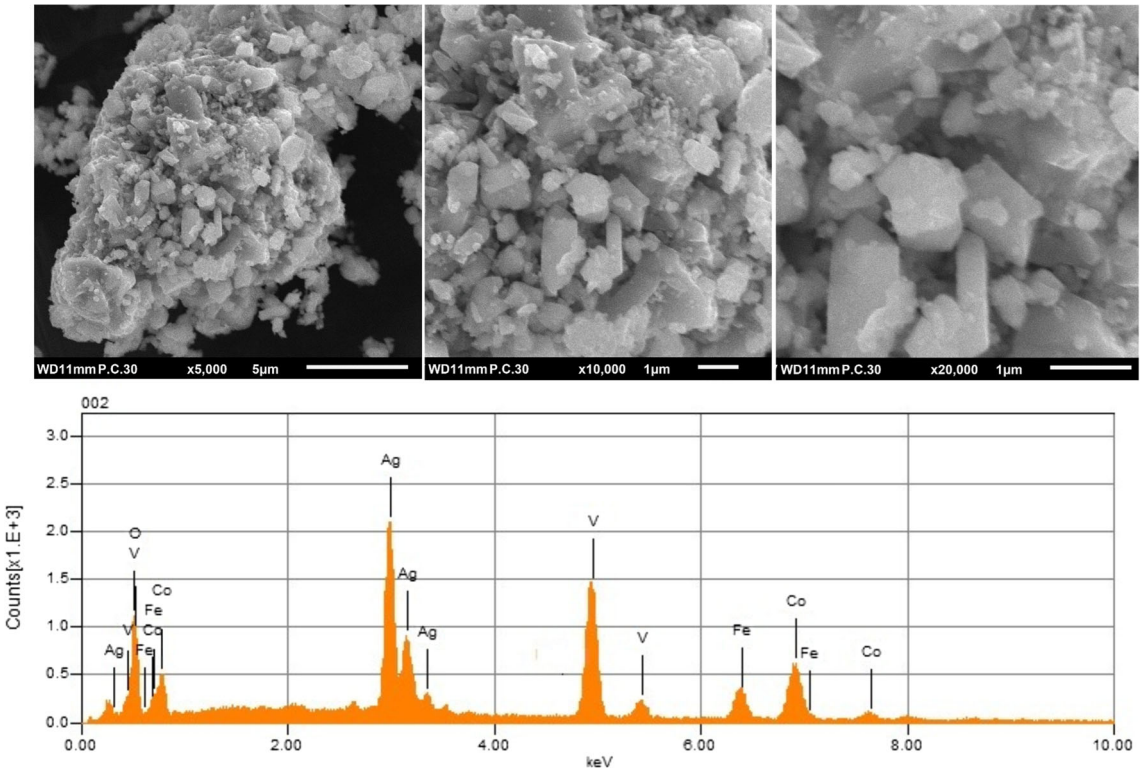

Fig. 2 SEM micrographs and EDS spectrum of the synthesized powder of $Ag_2Co_2Fe(VO_4)_3$

FT-infrared spectra of powder samples (in KBr pellet) were performed by an PerkinElmer RX-I model spectrometer with spectral resolution equal to 4 cm^{-1} over the entire frequency range of 400–1400 cm^{-1}.

2.2.3 Mössbauer Spectroscopy

To confirm the Fe^{III} oxidation state in the two vanadates, the Mössbauer spectra were recorded at room temperature in the standard transmission geometry, using a constant acceleration signal spectrometer equipped with Co^{57} source diffused into a rhodium matrix. Hyperfine parameters were calculated from the Mössbauer spectra using a least-squares method. Isomer shifts are reported relative to room temperature iron foil.

2.2.4 Magnetic Measurements

Magnetic measurements of $A_2Co_2Fe(VO_4)_3$ (A = Ag or Na) were performed by a Physical Property Measurement System (PPMS) DynaCool magnetometer on the synthesized powders sealed in a gelatin capsule. The temperature dependence magnetic susceptibility measurements were made between 300 and 2 K in both zero field cooled (ZFC) and filed cooled (FC) modes with an applied field 10 kOe. The ZFC mode

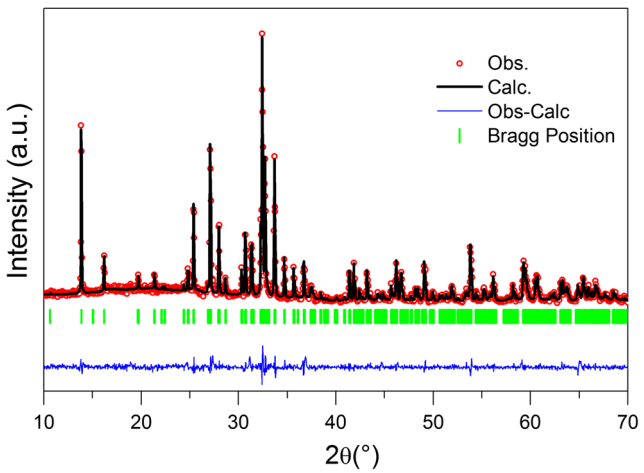

Fig. 3 Observed and refined PXRD patterns for $Na_2Co_2Fe(VO_4)_3$

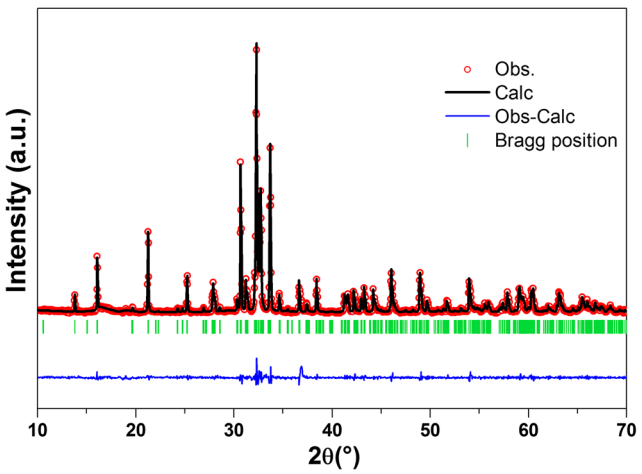

Fig. 4 Observed and refined PXRD patterns for $Ag_2Co_2Fe(VO_4)_3$

was performed by cooling the sample from 300 down to 2 K in the absence of a magnetic field. Subsequently, the desired external field was applied and the data were collected on heating the sample up to 300 K. After reaching 300 K, the data were then recorded with the same strength of the field on cooling the sample down to 2 K, i.e., FC.

3 Results and Discussion

3.1 Scanning Electron Microscopy and Powder X-Ray Diffraction

The morphology and elemental analysis of the synthesized powders of the two vanadates were characterized by scanning electron microscope (SEM) and energy-dispersive X-ray spectrometer (EDS) (see Figs. 1 and 2). The SEM images reveal the formation of particles with irregular shapes in the powder samples. The EDS analysis confirms the presence of only Fe, Co, V, Na, or Ag and oxygen atoms; also, Co/V, Fe/V, and Na/V or Ag/V ratios are close to those of the elemental composition. The purity of the as-synthesized powders was confirmed by powder X-ray diffraction. The obtained X-ray patterns were fitted using Le Bail refinement method with JANA2006 software [31, 32]. This refinement leads to good agreement between the experimental and the calculated patterns (Figs. 3 and 4), which confirms the single phase of the synthesized powders. The refined unit cell parameters are very close to those obtained from single crystal data [26]. Le Bail refinement parameters and unit cell parameters comparison with other homolog phosphates are presented in Table 1.

3.2 FT-IR and Raman Spectroscopy Results

The infrared and Raman spectra of the synthesized vanadates are plotted in Fig. 5. It has been reported in previous works on spectroscopy of vanadates [34–37] that isolated ion VO_4^{3-} with tetrahedral symmetry (T_d) is characterized by four vibrations: the ν_1 symmetric stretching mode Raman active observed around 878 cm^{-1}; the doubly degenerate ν_2 symmetric bending mode Raman active located around 345 cm^{-1}; the ν_3 triply degenerate antisymmetric stretching mode which is Raman and infrared active, observed at vicinity of 825 cm^{-1}; and the ν_4 triply degenerate antisymmetric bending mode which is also both Raman and infrared active, located around 480 cm^{-1}. When the symmetry becomes lower, the degeneracy is removed and all modes can become IR and Raman active [37].

For the vanadate $Na_2Co_2Fe(VO_4)_3$, as shown in Fig. 5a, the Raman bands at 897 and 827 cm^{-1} can be assigned to ν_1 the symmetric stretching vibration of VO_4^{3-}. The band observed

Table 1 Le Bail refinement parameters for $A_2Co_2Fe(VO_4)_3$ (A = Na and Ag) and lattice parameter comparison with analog phosphates

Chemical formula	$Na_2Co_2Fe(VO_4)_3$			$Ag_2Co_2Fe(VO_4)_3$	
Crystal system			Monoclinic		
Space group			*C2/c* (No 15)		
Refined unit cell parameters	$a = 11.7245$ (4) Å			$a = 11.7866$ (4) Å	
	$b = 12.7778$ (5) Å			$b = 12.8319$ (4) Å	
	$c = 6.8250$ (2) Å			$c = 6.8075$ (2) Å	
	$\beta = 111.022$ (2)°			$\beta = 110.966$ (2)°	
	$V = 954.43$ (7) $Å^3$			$V = 961.44$ (7) $Å^3$	
No. of data points	1501			1501	
No. of fitted parameters	9			9	
Profile function			Pseudo-Voigt		
Background			linear interpolation		
R-factors					
Rp	7.75			7.55	
Rwp	10.26			10.76	
Goodness of fit	1.34			1.36	
Lattice parameters comparison with other alluaudite phosphates					
Compound, ref.	*a* (Å)	*b* (Å)	c (Å)	*β* (°)	*V* ($Å^3$)
$Na_2Co_2Fe(VO_4)_3$, this work	11.7245 (4)	12.7778 (5)	6.8250 (2)	111.022 (2)	954.43 (7)
$Ag_2Co_2Fe(VO_4)_3$, this work	11.7866 (4)	12.8319 (4)	6.8075 (2)	110.966 (2)	961.44 (7)
$Na_2Co_2Fe(PO_4)_3$, [18]	11.7599 (3)	12.4522 (3)	6.4406 (2)	113.913 (2)	862.18 (4)
$Ag_{1.655}Co_{1.64}Fe_{1.36}(PO_4)_3$, [33]	11.8680 (3)	12.5514 (3)	6.4386 (2)	114.012 (1)	876.09 (4)

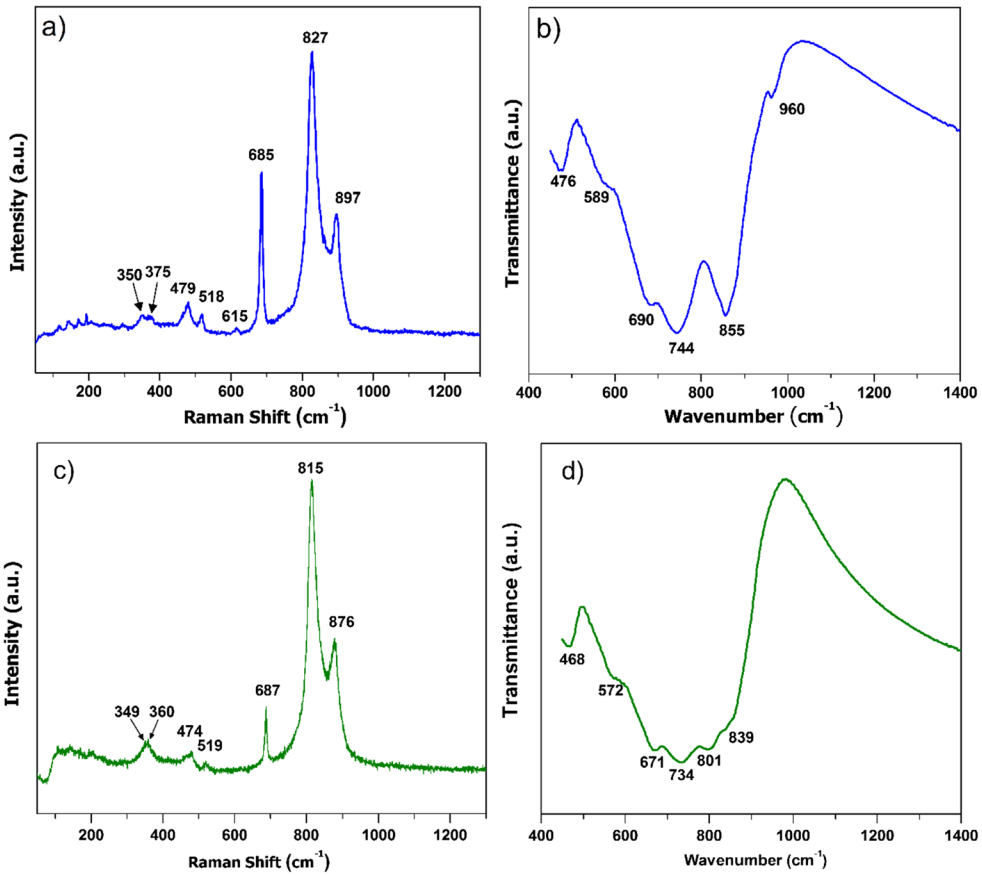

Fig. 5 Raman (**a**, **c**) and FT-IR spectra (**b**, **d**). The blue spectra are for $Na_2Co_2Fe(VO_4)_3$ and green ones for $Ag_2Co_2Fe(VO_4)_3$

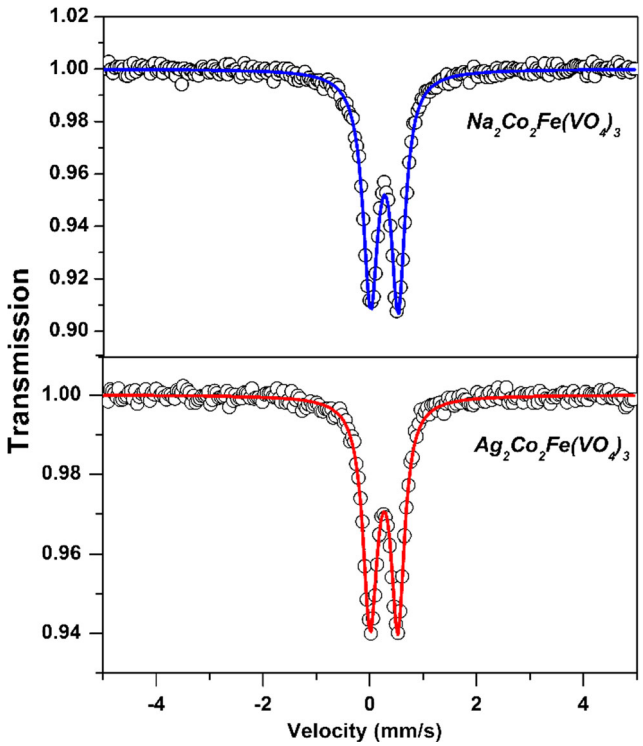

Fig. 6 Room temperature Mössbauer spectra of $A_2Co_2Fe(VO_4)_3$ (A = Ag or Na)

at 685 cm^{-1} and the very weak one at 615 cm^{-1} are most likely corresponding to ν_3 antisymmetric stretching vibration of VO_4^{3-}. The bands at 518 and 479 cm^{-1} are assigned to the ν_4 VO_4^{3-} antisymmetric bending mode, while the two bands at 375 and 350 cm^{-1} are ascribed to ν_2 VO_4^{3-} symmetric bending modes [38]. The observed weak bands at low frequency lower than 200 cm^{-1} are due to lattice vibrations. In the infrared spectrum (Fig. 5b), the located bands at 960, at 855, at 744 cm^{-1}, and at 690 cm^{-1} are assigned to ν_3 antisymmetric stretching modes of VO_4^{3-} [36]. The bands located at 589 cm^{-1} and at 476 cm^{-1} correspond to ν_4 antisymmetric bending mode of VO_4^{3-}.

For $Ag_2Co_2Fe(VO_4)_3$, in Fig. 5c, the Raman bands located at 876 and 815 cm^{-1} can be assigned to ν_1, the symmetric stretching vibration of VO_4^{3-}, which are shifted to lower frequency compares to the Na vanadate. This shift can be interpreted by the change of lattice parameters, i.e., the unit cell volume of the Ag vanadate is larger than that of the Na vanadate (see Table 1); consequently, the average

Table 2 Mössbauer spectral parameters for $A_2Co_2Fe(VO_4)_3$ (A = Ag or Na)

Compound	Site	δ (mm s^{-1})	Γ (mm s^{-1})	Δ (mm s^{-1})
$Na_2Co_2Fe(VO_4)_3$	$Fe^{3+}[O_h]$	0.37 (2)	0.33 (1)	0.52 (2)
$Ag_2Co_2Fe(VO_4)_3$	$Fe^{3+}[O_h]$	0.38 (2)	0.32 (2)	0.52 (1)

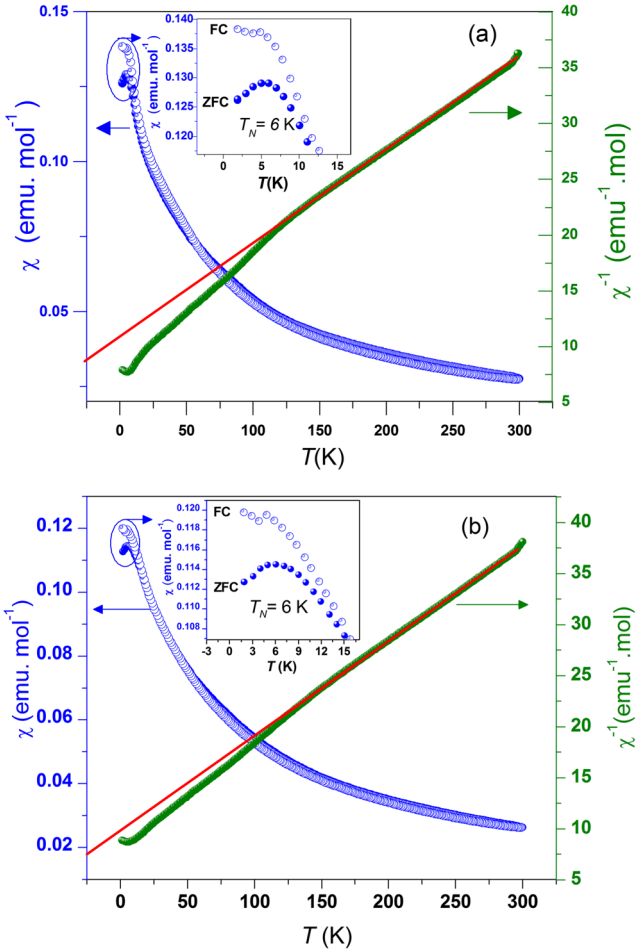

Fig. 7 Magnetic susceptibility in ZFC and FC modes and the inverse magnetic susceptibility of ZFC data **a** for $Na_2Co_2Fe(VO_4)_3$ and **b** for $Ag_2Co_2Fe(VO_4)_3$. The solid red line indicates the Curie–Weiss law fit. The inset plot shows the ordering temperature T_N and the deference between ZFC and FC curves

V–O distance for the Ag vanadate is slightly bigger [26]. The sharp band at 687 cm^{-1}, which is observed at 685 cm^{-1} in the sodium-based vanadate, corresponds to ν_3 antisymmetric stretching vibration of VO_4^{3-}. This band remains practically at the same frequency (very small shift to higher frequency); this can be explained by referring to the structural study of these two vanadates [26]: the distances V1–O2 and V1–O3 become slightly shorter in the Ag vanadate contrary to other V–O distances. The bands at 519 and 474 cm^{-1} are assigned to the ν_4 VO_4^{3-} antisymmetric bending modes, while the two bands at 360 and 349 cm^{-1} are assigned to ν_2 VO_4^{3-}symmetric bending modes [38]. The observed weak bands at low frequency lower than 200 cm^{-1} are due to lattice vibrations. In the infrared spectrum (Fig. 5d), the located bands at 839 cm^{-1}, at 801 cm^{-1}, at 734 cm^{-1}, and at 671 cm^{-1} correspond to the ν_3 VO_4^{3-} antisymmetric stretching vibrational mode [36]. The bands at 572 cm^{-1} and at 468 cm^{-1} are attributed to ν_4 antisymmetric bending mode VO_4^{3-}.

3.3 Mössbauer Spectroscopy

The ^{57}Fe Mössbauer spectra of the two compounds, recorded at room temperature, are presented in Fig. 6. Both spectra are in the form of a doublet justifying the paramagnetic character of these vanadates at room temperature. The continuous line represents result of the fitting procedure of the experimental data points shown as black circles. The fitting was performed using one distribution corresponding to a trivalent iron Fe^{3+} in the octahedral site. The hyperfine parameters obtained from this refinement, such as the isomeric shift (δ), the full width at half maximum (Γ), and the quadruple splitting (Δ), are listed in Table 2. The isomer shift values that are about 0.37 mm s^{-1} for $Na_2Co_2Fe(VO_4)_3$ and 0.38 mm s^{-1} for $Ag_2Co_2Fe(VO_4)_3$ are typical to high-spin Fe^{3+} in octahedral environment [39]. Indeed, paramagnetic spectra were observed in isostructural vanadates [27].

3.4 Magnetic Properties

Figure 7 shows the molar magnetic susceptibility (χ) and the inverse molar magnetic susceptibility χ^{-1} measured in both ZFC and FC modes with an applied field of 10 kOe for the two vanadates, within the temperature range of 2–300 K. The data were corrected from diamagnetic signal of all atoms (-203.6×10^{-6} emu mol^{-1} for $Na_2Co_2Fe(VO_4)_3$ and -246×10^{-6} emu mol^{-1} for $Ag_2Co_2Fe(VO_4)_3$). The high temperature region above 100 K of the inverse molar magnetic susceptibility versus T was fitted by the Curie–Weiss law, giving rise to a Curie−Weiss constant $\theta = -125.6$ K for $Na_2Co_2Fe(VO_4)_3$ and $\theta = -104.5$ K for $Ag_2Co_2Fe(VO_4)_3$ and to a Curie constant $C = 11.76$ emu K mol^{-1} and $C = 10.73$ emu K mol^{-1} per formula unit for $Na_2Co_2Fe(VO_4)_3$ and $Ag_2Co_2Fe(VO_4)_3$ respectively. The negative Curie–Weiss constants indicate that the predominant interactions are antiferromagnetic in both vanadates. The effective magnetic moment calculated from the Curie constant, μ_{eff} of 9.69 and 9.26 μ_B for $Na_2Co_2Fe(VO_4)_3$ and $Ag_2Co_2Fe(VO_4)_3$ respectively are in good agreement with the effective moment of $\mu_{eff} = 9.44$ μ_B expected from two high-spin Co^{2+} ($S = 3/2$) and one Fe^{3+} ($S = 5/2$) ions considering spin−orbit coupling hypothesis observed in Co^{2+} [40, 41]. The ordering temperature in both vanadates is observed at $T_N = 6$ K. As can be seen in the inset figures, the magnetic susceptibility for both vanadates presents remarkable divergence between ZFC and FC curves at very low temperature, suggesting the existence of a net uncompensated magnetic moment (weak ferromagnetism) [42–44]. In both vanadates, the Curie−Weiss constant $|\theta| >> T_N$ which is a sign of geometrical spin frustration [45]. Moreover, an empirical measure of frustration by calculating the quantity defined by Ramirez [45] is as follows: $f = -\theta_{cw}/T_N$, a value of $f > 10$ indicates strong frustration in the system. Accordingly, the calculated values of $f = 20.93$ for

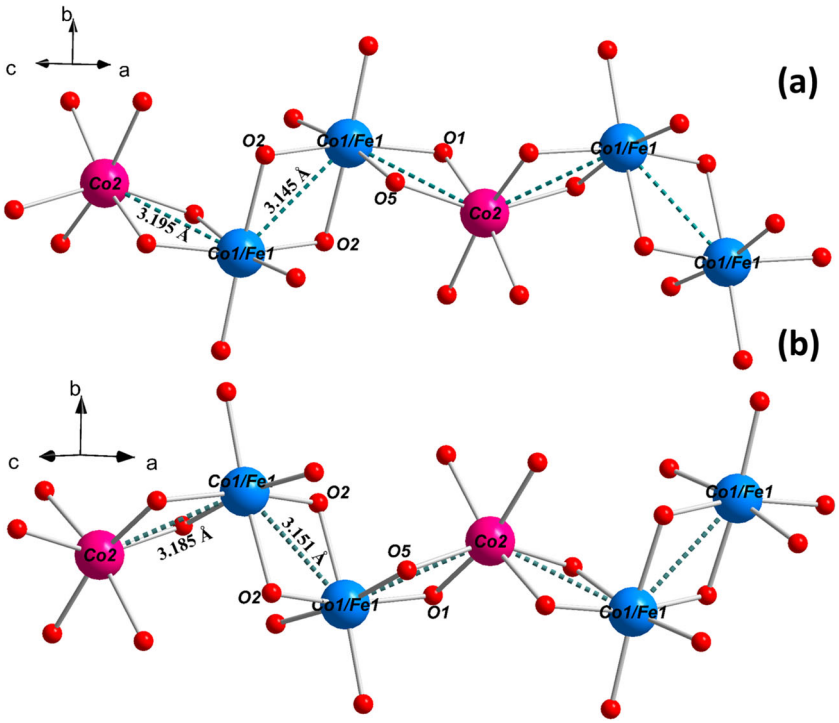

Fig. 8 Polyhedral representation showing the 90° cation–anion–cation interactions pathway along the [10$\bar{1}$] direction **a** in $Na_2Co_2Fe(VO_4)_3$ and **b** in $Ag_2Co_2Fe(VO_4)_3$

$Na_2Co_2Fe(VO_4)_3$ and $f = 17.41$ for $Ag_2Co_2Fe(VO_4)_3$ confirm the strong geometrical frustration in these two vanadates.

According to the structural study of these two vanadates $A_2Co_2Fe(VO_4)_3$ (A = Ag or Na) [26], the linkage of alternating $[CoO_6]$ octahedra and $[(Co,Fe)_2O_{10}]$ double octahedra through common edges leads to the formation of infinite chains running along the [10$\bar{1}$] direction (Fig. 8). These chains are connected by VO_4 tetrahedra to form layers parallel to the plane (101) (Fig. 9).

The superexchange magnetic interactions in these two vanadates can be discussed with reference to Goodenough–Kanamori–Anderson (GKA) semiempirical rules [46–48]. In the chains, two types of superexchange interactions are possible: the first one occurs between mixed sites of the dimers $[(Co, Fe)_2O_{10}]$. The distance between the centers of these mixed sites is 3.145 Å for Na vanadate and 3.151 Å for Ag vanadate and the angle (Co1/Fe1)–O–(Co1/Fe1) is 96.28 ° and 96.94° for the Na vanadate and that of Ag respectively. This connection suggests the existence of a competition between three possible 90 ° cation–anion–cation interactions in these dimers, Fe^{3+}–O3–Fe^{3+}, Co^{2+}–O3–Fe^{3+}, and Co^{2+}–O3–Co^{2+} (see Fig. 8). By referring to GKA rules [46–48], the direct interactions 90 ° Fe^{3+}–O3–Fe^{3+} are antiferromagnetic, whereas the 90 ° interactions of Co^{2+}–O3–Fe^{3+} and Co^{2+}–O3–Co^{2+} should be ferromagnetic.

Also, the second type of interaction arises between the $Co(2)O_6$ octahedra and the mixed-occupied $(Co(1)/Fe(1))O_6$ octahedra linked through edge sharing made by O1 and O5 atoms, as shown in Fig. 8, which gives two type of 90° cation–anion–cation interactions, Co^{2+}–O–

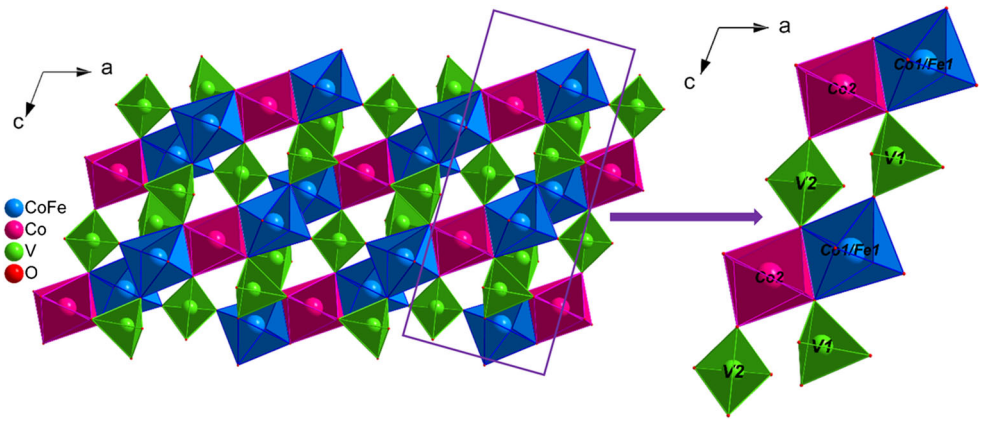

Fig. 9 Polyhedral representation showing the two 180° cation–anion–anion–cation superexchange pathways along the [001]. Data from $Na_2Co_2Fe(VO_4)_3$

Fe^{3+} and Co^{2+}–O–Co^{2+}, expected as ferromagnetic interactions. The distance between Co(2)–(Co(1)/Fe(1)) is 3.195 (1) Å and 3.185 (1) Å for the Na and Ag phases respectively. The angle (Co1/Fe1)–O1–Co(2) is 100.59 (1)° and 100.25 (1)° for Na and Ag vanadate respectively, while the angle (Co1/Fe1)–O5–Co(2) is 101.25 (1)° and 101.17 (1)° for Na and Ag phases respectively. It is worthy to mention that the side groups attached to bridging anions, which are in our case VO_4^{3-}, may reverse the sign of the 90° superexchange as reported by Geertsma and Khomskii [49].

In addition to the above interactions which takes into account the interactions inside the chains, a second type of interactions that manifests itself between the chains is expected. These interactions are of cation–anion–anion–cation type, which occur between $(Co(1)/Fe(1))O_6$ octahedra via $V(1)O_4$ tetrahedron and between $Co(2)O_6$ octahedra through $V(2)O_4$ tetrahedron in [001] direction (Fig. 9). These type of superexchange interaction follow the same rules as those of 180° cation–anion–cation which gives according to Goodenough–Kanamori–Anderson rules antiferromagnetic interactions in case of Co^{2+}–O–O–Fe^{3+}, Co^{2+}–O–O–Co^{2+} and Fe^{3+}–O–O–Fe^{3+} superexchange interactions.

In summary, in the chains of these two vanadates, the magnetic superexchange interactions according to the GKA rules are in competition between the antiferromagnetic state and the ferromagnetic state, whereas the inter-chain interactions are antiferromagnetic. Thus, the dominant interactions in these two vanadates are antiferromagnetic which is consistent with the experimental results.

4 Conclusion

The powders of the two vanadates, $A_2Co_2Fe(VO_4)_3$ (A = Ag or Na), were synthesized using sol–gel method and characterized by powder X-ray diffraction, scanning electron microscopy, IR and Raman spectroscopies, Mössbauer spectroscopy, and magnetic measurements. The magnetic susceptibility data confirmed that the predominant interaction is antiferromagnetic with a Curie–Weiss constant of $\theta = -125.6$ K for $Na_2Co_2Fe(VO_4)_3$ and $\theta = -104.5$ K for $Ag_2Co_2Fe(VO_4)_3$. The magnetic transition from the paramagnetic state to the antiferromagnetic state is observed around 6 K in both vanadates. The temperature dependence magnetic susceptibility measurements at 10 kOe in both ZFC and FC modes show divergence in the curves for both vanadates at low temperature, indicating the presence of weak ferromagnetism. The high $-\theta_{cw}/T_N$ ratio confirms the existence strong geometrical frustration in these two vanadates. The super exchange interactions according to GKA rules confirm that the expected over all magnetic interactions are antiferromagnetic consistently with the experimental findings.

Funding Information This work was done with the support of CNRST (Centre National pour la Recherche Scientifique et Technique) in the Excellence Research Scholarships Program.

Compliance with Ethical Standards

Conflict of Interest The authors declare that they have no conflict of interest.

References

1. Guo, S.-P., Li, J.-C., Xu, Q.-T., Ma, Z., Xue, H.-G.: Recent achievements on polyanion-type compounds for sodium-ion batteries: syntheses, crystal chemistry and electrochemical performance. J. Power Sources. **361**, 285–299 (2017). https://doi.org/10.1016/j.jpowsour.2017.07.002
2. Masquelier, C., Croguennec, L.: Polyanionic (phosphates, silicates, sulfates) frameworks as electrode materials for rechargeable Li (or Na) batteries. Chem. Rev. **113**, 6552–6591 (2013). https://doi.org/10.1021/cr3001862
3. Clearfield, A., Thakur, D.S.: Zirconium and titanium phosphates as catalysts: a review. Appl. Catal. **26**, 1–26 (1986). https://doi.org/10.1016/S0166-9834(00)82538-5
4. Ghiyasiyan-Arani, M., Masjedi-Arani, M., Salavati-Niasari, M.: Size controllable synthesis of cobalt vanadate nanostructures with enhanced photocatalytic activity for the degradation of organic dyes. J. Mol. Catal. Chem. **425**, 31–42 (2016). https://doi.org/10.1016/j.molcata.2016.09.023
5. Natarajan, S., Mandal, S.: Open-framework structures of transition-metal compounds. Angew. Chem. Int. Ed. **47**, 4798–4828 (2008). https://doi.org/10.1002/anie.200701404
6. Cheetham, A.K., Férey, G., Loiseau, T.: Open-framework inorganic materials. Angew. Chem. Int. Ed. **38**, 3268–3292 (1999). https://doi.org/10.1002/(SICI)1521-3773(19991115)38:22<3268::AID-ANIE3268>3.0.CO;2-U
7. Moore, P.B.: Crystal chemistry of the alluaudite structure type: contribution to the para-genesis of pegmatite phosphate giant crystals. Am. Mineral. **56**, 1955–1975 (1971)
8. Hatert, F., Fransolet, A.-M., Maresch, W.V.: The stability of primary alluaudites in granitic pegmatites: an experimental investigation of the $Na_2(Mn_{2-2x}Fe_{1+2x})(PO_4)_3$ system. Contrib. Mineral. Petrol. **152**, 399–419 (2006). https://doi.org/10.1007/s00410-006-0115-2
9. Khmiyas, J., Assani, A., Saadi, M., El Ammari, L.: Crystal structure of a sodium, zinc and iron(III)-based non-stoichiometric phosphate with an alluaudite-like structure: $Na_{1.67}$ $Zn_{1.67}Fe_{1.33}(PO_4)_3$. Acta Crystallogr. Sect. E Crystallogr. Commun. **71**, 690–692 (2015). https://doi.org/10.1107/S2056989015009767
10. Assani, A., Saadi, M., Zriouil, M., El Ammari, L.: Silver trimagnesium phosphate bis(hydrogenphosphate), $AgMg_3(PO_4)(HPO_4)_2$, with an alluaudite-like structure. Acta Crystallogr. Sect. E Struct. Rep. Online. **67**, i5 (2011). https://doi.org/10.1107/S1600536810053304
11. Kim, J., Kim, H., Lee, S., Myung, S.-T.: Development of a new alluaudite-based cathode material with high power and long cyclability for application in Na ion batteries in real-life. J. Mater. Chem. A. **5**, 22334–22340 (2017). https://doi.org/10.1039/C7TA06693G
12. Karegeya, C., Mahmoud, A., Vertruyen, B., Hatert, F., Hermann, R.P., Cloots, R., Boschini, F.: One-step hydrothermal synthesis and

electrochemical performance of sodium-manganese-iron phosphate as cathode material for Li-ion batteries. J. Solid State Chem. **253**, 389–397 (2017). https://doi.org/10.1016/j.jssc.2017.06.021
13. Fisher, D.J.: Alluaudite. Am. Mineral. **40**, 1100–1109 (1955)
14. Hatert, F., Keller, P., Lissner, F., Antenucci, D., Fransolet, A.-M.: First experimental evidence of alluaudite-like phosphates with high Li-content: the $(Na_{1-x}Li_x)MnFe_2(PO_4)_3$ series (x = 0 to 1). Eur. J. Mineral. **12**, 847–857 (2000)
15. Hatert, F.: Crystal chemistry of the divalent cation in alluaudite-type phosphates: a structural and infrared spectral study of the $Na_{1.5}(Mn_{1-x}M_{2+x})_{1.5}Fe_{1.5}(PO_4)_3$ solid solutions (x = 0 to 1, M^{2+} = Cd^{2+}, Zn^{2+}). J. Solid State Chem. **181**, 1258–1272 (2008). https://doi.org/10.1016/j.jssc.2008.02.035
16. Hatert, F.: Crystal chemistry of the hydrothermally synthesized $Na_2(Mn_{1-x}Fe_x^{2+})_2Fe^{3+}(PO_4)_3$ alluaudite-type solid solution. Am. Mineral. **90**, 653–662 (2005). https://doi.org/10.2138/am.2005.1551
17. Karegeya, C., Mahmoud, A., Hatert, F., Vertruyen, B., Cloots, R., Lippens, P.-E., Boschini, F.: $Na_{1.25}Ni_{1.25}Fe_{1.75}(PO_4)_3$ nanoparticles as a janus electrode material for Li-ion batteries. J. Power Sources. **388**, 57–64 (2018). https://doi.org/10.1016/j.jpowsour.2018.03.069
18. Essehli, R., Belharouak, I., Ben Yahia, H., Maher, K., Abouimrane, A., Orayech, B., Calder, S., Zhou, X.L., Zhou, Z., Sun, Y.-K.: Alluaudite $Na_2Co_2Fe(PO_4)_3$ as an electroactive material for sodium ion batteries. Dalton Trans. **44**, 7881–7886 (2015). https://doi.org/10.1039/C5DT00971E
19. Essehli, R., Ben Yahia, H., Maher, K., Sougrati, M.T., Abouimrane, A., Park, J.-B., Sun, Y.-K., Al-Maadeed, M.A., Belharouak, I.: Unveiling the sodium intercalation properties in $Na_{1.86}\square_{0.14}Fe_3(PO_4)_3$. J. Power Sources. **324**, 657–664 (2016). https://doi.org/10.1016/j.jpowsour.2016.05.125
20. Liu, D., Palmore, G.T.R.: Synthesis, crystal structure, and electrochemical properties of alluaudite $Na_{1.702}Fe_3(PO_4)_3$ as a sodium-ion battery cathode. ACS Sustain. Chem. Eng. **5**, 5766–5771 (2017). https://doi.org/10.1021/acssuschemeng.7b00371
21. Hadouchi, M., Assani, A., Saadi, M., Saadoune, I., Lahmar, A., Bouyanfif, H., El Marssi, M., El Ammari, L.: Synthesis, crystal structure and properties of a new phosphate, $Na_2Co_2Cr(PO_4)_3$. J. Inorg. Organomet. Polym. Mater. **28**, 2854–2864 (2018). https://doi.org/10.1007/s10904-018-0956-y
22. Chouaibi, N., Daidouh, A., Pico, C., Santrich, A., Veiga, M.L.: Neutron diffraction, Mössbauer spectrum, and magnetic behavior of $Ag_2FeMn_2(PO_4)_3$ with alluaudite-like structure. J. Solid State Chem. **159**, 46–50 (2001). https://doi.org/10.1006/jssc.2001.9128
23. Stock, N., Stucky, G., Cheetham, A.: Influence of the cation size on the formation of alluaudite-type manganese arsenates: synthesis and characterization of $Tl_2Mn_3(As_2O_7)_2\cdot 2H_2O$, $CsMn_3(AsO_4)(HAsO_4)_2\cdot 3H_2O$, and $XMn_3(AsO_4)(HAsO_4)_2$ (X = Na, K). J. Phys. Chem. Solids. **62**, 1457–1467 (2001). https://doi.org/10.1016/S0022-3697(01)00062-2
24. Krivovichev, S.V., Vergasova, L.P., Filatov, S.K., Rybin, D.S., Britvin, S.N., Ananiev, V.V.: Hatertite, $Na_2(Ca, Na)(Fe^{3+}, Cu)_2(AsO_4)_3$, a new alluaudite-group mineral from Tolbachik fumaroles, Kamchatka peninsula, Russia. Eur. J. Mineral. **25**, 683–691 (2013). https://doi.org/10.1127/0935-1221/2013/0025-2311
25. Dwibedi, D., Ling, C.D., Araujo, R.B., Chakraborty, S., Duraisamy, S., Munichandraiah, N., Ahuja, R., Barpanda, P.: Ionothermal synthesis of high-voltage alluaudite $Na_{2+2x}Fe_{2-x}(SO_4)_3$ sodium insertion compound: structural, electronic, and magnetic insights. ACS Appl. Mater. Interfaces. **8**, 6982–6991 (2016)
26. Hadouchi, M., Assani, A., Saadi, M., El Ammari, L.: The alluaudite-type crystal structures of $Na_2(Fe/Co)_2Co(VO_4)_3$ and $Ag_2(Fe/Co)_2Co(VO_4)_3$. Acta Crystallogr. Sect. E Crystallogr. Commun. **72**, 1017–1020 (2016). https://doi.org/10.1107/S2056989016009981
27. Ben Yahia, H., Shikano, M., Tabuchi, M., Belharouak, I.: Synthesis, crystal structure, and properties of the alluaudite-type vanadates $Ag_{2-x}Na_xMn_2Fe(VO_4)_3$. Inorg. Chem. **55**, 4643–4649 (2016). https://doi.org/10.1021/acs.inorgchem.6b00486
28. Lamsakhar, N.E.H., Zriouil, M., Assani, A., Saadi, M., El Ammari, L.: Crystal structure of disilver(I) dizinc(II) iron(III) tris(orthovanadate) with an alluaudite-type structure. Acta Crystallogr. Sect. E Crystallogr. Commun. **74**, 1155–1158 (2018). https://doi.org/10.1107/S205698901801071X
29. Essehli, R., Bali, B.E., Benmokhtar, S., Bouziane, K., Manoun, B., Abdalslam, M.A., Ehrenberg, H.: Crystal structures and magnetic properties of iron (III)-based phosphates: $Na_4NiFe(PO_4)_3$ and $Na_2Ni_2Fe(PO_4)_3$. J. Alloys Compd. **509**, 1163–1171 (2011). https://doi.org/10.1016/j.jallcom.2010.08.159
30. Leroux, F., Mar, A., Payen, C., Guyomard, D., Verbaere, A., Piffard, Y.: Synthesis and structure of $NaMn_3(PO_4)(HPO_4)_2$, an unoxidized variant of the alluaudite structure type. J. Solid State Chem. **115**, 240–246 (1995). https://doi.org/10.1006/jssc.1995.1127
31. Le Bail, A.: Whole powder pattern decomposition methods and applications: a retrospection. Powder Diffract. **20**, 316–326 (2005). https://doi.org/10.1154/1.2135315
32. Petříček, V., Dušek, M., Palatinus, L.: Crystallographic computing system JANA2006: general features. Z. Für Krist. - Cryst. Mater. **229**, (2014). https://doi.org/10.1515/zkri-2014-1737
33. Bouraima, A., Makani, T., Assani, A., Saadi, M., El Ammari, L.: Crystal structure of a silver-, cobalt- and iron-based phosphate with an alluaudite-like structure: $Ag_{1.655}Co_{1.64}Fe_{1.36}(PO_4)_3$. Acta Crystallogr. Sect. E Crystallogr. Commun. **73**, 890–892 (2017). https://doi.org/10.1107/S205698901700740X
34. Ross, S.D.: Inorganic Infrared and Raman Spectra. McGraw-Hill, London (1972)
35. Farmer, V.C. (ed.): The Infrared Spectra of Minerals. Mineralogical Society, London (1974)
36. Busca, G., Ricchiardi, G., Sam, D.S.H., Volta, J.-C.: Spectroscopic characterization of magnesium vanadate catalysts. Part 1.—Vibrational characterization of $Mg_3(VO_4)_2$, $Mg_2V_2O_7$ and MgV_2O_6 powders. J Chem Soc Faraday Trans. **90**, 1161–1170 (1994). https://doi.org/10.1039/FT9949001161
37. Busca, G.: Differentiation of mono-oxo and polyoxo and of monomeric and polymeric vanadate, molybdate and tungstate species in metal oxide catalysts by IR and Raman spectroscopy. J. Raman Spectrosc. **33**, 348–358 (2002). https://doi.org/10.1002/jrs.867
38. Frost, R.L., Palmer, S.J., Čejka, J., Sejkora, J., Plášil, J., Bahfenne, S., Keeffe, E.C.: A Raman spectroscopic study of the different vanadate groups in solid-state compounds-model case: mineral phases vésigniéite $[BaCu_3(VO_4)_2(OH)_2]$ and volborthite $[Cu_3V_2O_7(OH)_2\cdot 2H_2O]$. J. Raman Spectrosc. **42**, 1701–1710 (2011). https://doi.org/10.1002/jrs.2906
39. Menil, F.: Systematic trends of the 57Fe Mössbauer isomer shifts in (FeOn) and (FeFn) polyhedra. Evidence of a new correlation between the isomer shift and the inductive effect of the competing bond T-X (→ Fe) (where X is O or F and T any element with a formal positive charge). J. Phys. Chem. Solids. **46**, 763–789 (1985). https://doi.org/10.1016/0022-3697(85)90001-0
40. Ostrovsky, S.M., Falk, K., Pelikan, J., Brown, D.A., Tomkowicz, Z., Haase, W.: Orbital angular momentum contribution to the magneto-optical behavior of a binuclear cobalt(II) complex. Inorg. Chem. **45**, 688–694 (2006). https://doi.org/10.1021/ic0514748
41. Zarembowitch, J., Kahn, O.: Magnetic properties of some spin-crossover, high-spin, and low-spin cobalt(II) complexes with Schiff bases derived from 3-formylsalicylic acid. Inorg. Chem. **23**, 589–593 (1984). https://doi.org/10.1021/ic00173a020
42. Moriya, T.: Anisotropic superexchange interaction and weak ferromagnetism. Phys. Rev. **120**, 91–98 (1960). https://doi.org/10.1103/PhysRev.120.91

43. Zheng, L.-M., Gao, S., Yin, P., Xin: One-dimensional cobalt diphosphonates exhibiting weak ferromagnetism and field-induced magnetic transitions. Inorg. Chem. **43**, 2151–2156 (2004). https://doi.org/10.1021/ic034614r
44. Lu, Y.-B., Wang, M.-S., Zhou, W.-W., Xu, G., Guo, G.-C., Huang, J.-S.: Novel 3-D PtS-like tetrazolate-bridged manganese(II) complex exhibiting spin-canted antiferromagnetism and field-induced spin-flop transition. Inorg. Chem. **47**, 8935–8942 (2008). https://doi.org/10.1021/ic801026y
45. Ramirez, A.P.: Strongly geometrically frustrated magnets. Annu. Rev. Mater. Sci. **24**, 453–480 (1994). https://doi.org/10.1146/annurev.ms.24.080194.002321
46. Kanamori, J.: Superexchange interaction and symmetry properties of electron orbitals. J. Phys. Chem. Solids. **10**, 87–98 (1959). https://doi.org/10.1016/0022-3697(59)90061-7
47. Anderson, P.W.: New approach to the theory of superexchange interactions. Phys. Rev. **115**, 2–13 (1959). https://doi.org/10.1103/PhysRev.115.2
48. Goodenough, J.B.: Magnetism and the Chemical Bond. Wiley, NY-London (1963)
49. Geertsma, W., Khomskii, D.: Influence of side groups on 90° superexchange: a modification of the Goodenough-Kanamori-Anderson rules. Phys. Rev. B. **54**, 3011–3014 (1996). https://doi.org/10.1103/PhysRevB.54.3011